Waveguide measurements of the permittivity and permeability at temperatures up to 1000 C

Larsson, Christer; Sjöberg, Daniel; Elmkvist, Lisa

2010

CODEN:LUTEDX/(TEAT-7196)/1-22/(2010)

Waveguide measurements of the permittivity and permeability at temperatures up to $1000\,^{\circ}\mathrm{C}$

Christer Larsson, Daniel Sjöberg, and Lisa Elmkvist

Electromagnetic Theory
Department of Electrical and Information Technology
Lund University
Sweden

Christer Larsson
Christer.Larsson@saabgroup.com and Christer.Larsson@eit.lth.se

Saab Dynamics AB
SE-581 88 Linköping
Sweden

Department of Electrical and Information Technology
Electromagnetic Theory
Lund University
P.O. Box 118
SE-221 00 Lund
Sweden

Daniel Sjöberg
Daniel.Sjoberg@eit.lth.se

Department of Electrical and Information Technology
Electromagnetic Theory
Lund University
P.O. Box 118
SE-221 00 Lund
Sweden

Lisa Elmkvist
Lisa.Elmkvist@exova.com

Exova AB
P.O. Box 1340
SE-581 13 Linköping
Sweden

Editor: Gerhard Kristensson

Abstract

This paper describes a method to measure the permittivity and the permeability at temperatures from room temperature up to 1000 °C using a single rectangular waveguide. The hardware design of the setup that can handle these temperatures and the procedure that is required to correct for the thermal expansion is developed. This includes the sample displacement, the displacement of the calibration reference planes, the thermal expansion of the waveguide and the gap between the sample and the waveguide wall. Measurements on Macor® and NiZn Ferrite samples are performed in order to evaluate the performance of the setup and the procedure that is used to determine the permittivity and permeability from the measured S-parameters.

1 Introduction

Accurate values for the high temperature permittivity and permeability at microwave frequencies are crucial for many applications. One example is for the modeling of microwave heating systems where it is important to have an accurate knowledge of the complex dielectric constant for the heated material [19]. Another example is the electromagnetic properties of radome materials on aircraft and missiles. The radome material is heated aerodynamically and the properties change with temperature [7]. It is then important that the designers of the radomes have access to these data, *e.g.*, so that radiation patterns can be modeled accurately.

A common way of determining the electromagnetic properties of materials is to use a rectangular waveguide. A sample, a rectangular piece of the material to be investigated, is then inserted in the waveguide and the transmission and reflection *i.e.*, the S-parameters, are measured. The electromagnetic material parameters, the complex-valued permittivity, ϵ and permeability, μ for the material can then be determined from the measurement using an inversion algorithm.

Several procedures have been developed for the inversion where the measured S-parameters are used to obtain ϵ and μ. The Nicolson-Ross-Weir [20, 27] (NRW) method is commonly used for this inversion. An alternate way of performing the inversion is to use a physically realistic model with adjustable parameters that obey causality for the frequency dependent ϵ and μ such as one or several Debye or Lorentz type models. The material parameters ϵ and μ are then obtained using an optimization procedure [2].

There are practical advantages of using rectangular waveguide measurements. Perhaps most important is the ease of sample manufacturing and that the sample is relatively small, compared to a free space measurement, which is important when only small amounts of the material is available for technical or economic reasons. These advantages of the rectangular waveguide measurements are valid for high temperatures also. However, using a waveguide for significantly higher temperatures than room temperature is not without complications. First of all, the waveguide material has to withstand the temperature. Secondly, the thermal expansion of the waveguide and the sample have to be corrected for. The thermal effects cause displacements of the S-parameter reference planes, a change in the

width of the waveguide leading to a change in the waveguide propagation. In addition, the thickness of the sample changes.

An alternative to using a rectangular waveguide is to perform a free space measurement on a sample placed between two antennas combined with focusing lenses. The advantage of such a setup is that the sample is not in thermal contact with the more sensitive microwave part of the instrumentation. Measurements of the permittivity of different materials at temperatures up to 850 °C [26] and up to 1600 °C [12] are reported using free space methods. The main disadvantage is the relatively large samples that are needed when using this method.

Another alternative is to use an open ended coaxial line where the end of the probe is inserted into an oven containing the sample while the part of the coaxial line that is outside the oven is cooled using a water jacket. Measurement at temperatures up to 800 °C can be made [1]. The disadvantages are similar to when using a rectangular waveguide since parts of the probe are heated.

A cavity resonator with two dominating modes is used in another study to measure the dielectric properties of materials. One mode is used to heat the sample and the other mode is used to perform the measurement of the dielectric constant. Since the heating is very rapid the measurement cell remains close to room temperature through the measurement for sample temperatures up to 1500 °C [8].

There are some previous studies where waveguide measurements are used to measure the electromagnetic material parameters at high temperature. In one study a rectangular waveguide is used to measure the X-band dielectric properties for alumina and silicon nitride for temperatures in the range 22 °C to 900 °C and a coax fixture is used for 2-18 GHz for the temperature range 25 °C to 500 °C. The advantages of the coax and rectangular waveguide fixtures are compared. The main advantages of the coax fixture are the large bandwidth for the measurement and the simple air gap correction. The disadvantages of the coax fixture are the sample shape, some issues with the center conductor and the sensitivity of the dimensions. Details on the materials used in the waveguide and coax fixtures are not disclosed [11].

An innovative design is used in another study employing a dual X-band waveguide manufactured from Inconel alloy 601® [4]. The waveguide is placed in an oven capable of heating the waveguide with the sample up to 1093 °C. One of the two parallel waveguide arms is used for the sample while the other arm is measured to obtain reference data for the phase changes that are caused by the thermal expansion of the fixture. Both the permittivity and permeability are measured for different materials [4].

In this paper we describe a method to determine the permittivity and permeability at temperatures from 22 °C to 1000 °C using a single waveguide setup. The heated parts of the waveguide fixture are manufactured from Inconel alloy 600®. The S-parameters are measured and the NRW inversion method is used in order to determine ϵ and μ. The thermal expansion causes displacements of the reference planes for the S-parameters, which are accounted for by performing separate compensation measurements. Tabulated data for the thermal expansion of the waveguide and the sample are used to determine the changes in the width of the waveguide

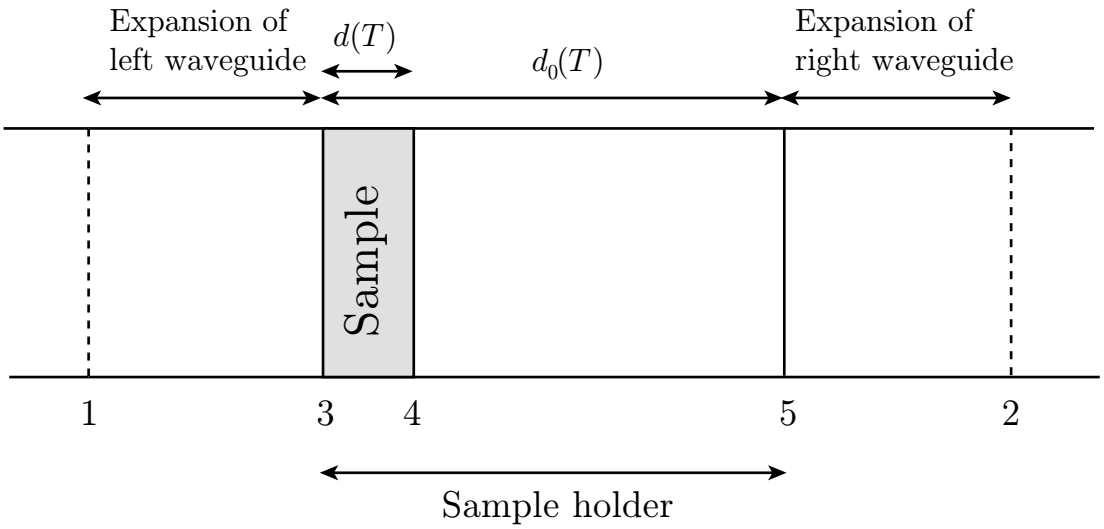

Figure 1: Reference planes. Planes 1 and 2 are the calibration planes, 3 and 5 are the sample holder edges, 3 and 4 are the sample edges.

that influences the waveguide propagation and the thickness of the sample. Furthermore, when the waveguide material has a larger thermal expansion coefficient than the sample material a gap is formed between the sample and the waveguide wall. The effect of this gap on the electromagnetic material parameters can also be accounted for. The setup is presently hardware limited to X-band measurements but can be easily extended to waveguide measurements for other bands and for coax transmission line measurements.

2 Theory

2.1 The Nicholson-Ross-Weir inversion method

The sample with thickness d is placed in a waveguide with width a and height b. The complex valued S-parameters are obtained by a vector network analyzer measurement. The NRW method [20, 27] is then performed using the following steps. First, define K as

$$K = \frac{r^2 - t^2 + 1}{2r}, \tag{2.1}$$

where r is the complex reflection scattering parameter and t is the complex transmission scattering parameter, corresponding to the measured S_{11} and S_{21} parameters with the reference phase planes at the surfaces of the sample. For reciprocal materials, the equation (2.1) and the following relations are also valid for incidence from the opposite direction, *i.e.*, by using S_{22} and S_{12} for r and t with the proper positioning of the reference planes. The interface reflection coefficient, Γ, is then given by

$$\Gamma = K \pm \sqrt{K^2 - 1} \tag{2.2}$$

where the sign is chosen according to the condition $|\Gamma| \leq 1$. The propagation factor P is then given by

$$P = \frac{r + t + \Gamma}{1 - (r + t)\,\Gamma} \tag{2.3}$$

The propagation factor can also be written as a function of the electromagnetic material parameters

$$P = \exp(-\mathrm{j}\beta d) \tag{2.4}$$

where d is the thickness of the slab and β is defined by

$$\beta = \sqrt{k_0^2 \epsilon\mu - k_\mathrm{c}^2} \tag{2.5}$$

where $k_0 = 2\pi/\lambda_0$ is the wave number in vacuum and $k_c = 2\pi/\lambda_c$ is the wave number at the cutoff wavelength $\lambda_c = 2a$. Having determined P from (2.3) one can solve for the argument in (2.4) by writing

$$\phi = \ln\left(\frac{1}{P}\right) + \mathrm{j}m2\pi, \tag{2.6}$$

where $\phi = \mathrm{j}\beta d$ and ln is the standard complex logarithmic function with branch cut at the negative real axis. The extra term $\mathrm{j}m2\pi$ reflects the periodicity of the exponential function, and the number m is determined at each frequency by phase unwrapping, starting with $m = 0$ at low frequencies where the sample is electrically thin. This gives the following expression for β

$$\beta = \frac{-\mathrm{j}\phi}{d}. \tag{2.7}$$

When β thus is known (2.5) can be rewritten to determine the product of ϵ and μ

$$\epsilon\mu = \frac{\beta^2 + k_\mathrm{c}^2}{k_0^2} \tag{2.8}$$

If the measured material is known to have no magnetic properties the permeability can be set to $\mu = 1$. In that case (2.8) can be used to solve directly for ϵ. In the general case when the magnetic properties of the material are not fully known, μ is given by

$$\mu = \frac{\beta}{\beta_0}\left(\frac{1 + \Gamma}{1 - \Gamma}\right) \tag{2.9}$$

where β_0 is given by

$$\beta_0 = \sqrt{k_0^2 - k_\mathrm{c}^2} \tag{2.10}$$

The permittivity ϵ is obtained by combining (2.8) and (2.9).

2.2 Correcting for reference plane displacement

In order to acquire a set of data to use for temperature compensation the reflection and the line standard are measured at several temperatures. The S-parameters obtained in the compensation data measurements are denoted $S^{\mathrm{R}}(T)$ and $S^{\mathrm{L}}(T)$, respectively. The S-parameters, $S(T)$, are then measured at the desired temperatures.

The task ahead is then to transfer the reference planes of the scattering parameters for the material data from planes 1 and 2 in Figure 1 to planes 3 and 4. This can be done in the following way. The primes indicate a reference plane from the right, and T_0 is the reference temperature where the calibration is made.

$$r_{\mathrm{left}}(T) = S_{33}(T) = S_{11}(T)\frac{-S^{\mathrm{R}}_{11}(T_0)}{-S^{\mathrm{R}}_{11}(T)} \tag{2.11}$$

$$t_{\mathrm{left}}(T) = S_{43}(T) = \mathrm{e}^{-\mathrm{j}\beta_0(T)d(T)}\underbrace{S_{21}(T)\frac{1}{S^{\mathrm{L}}_{21}(T)}}_{=S_{1'1}(T)} \tag{2.12}$$

$$\begin{aligned} r_{\mathrm{right}}(T) = S_{4'4'}(T) &= \mathrm{e}^{-2\mathrm{j}\beta_0(T)d(T)}S_{3'3'}(T) \\ &= \mathrm{e}^{-2\mathrm{j}\beta_0(T)d(T)}\underbrace{S_{22}(T)\frac{1}{S^{\mathrm{L}}_{21}(T)S^{\mathrm{L}}_{12}(T)}}_{=S_{1'1'}(T)}\frac{-S^{\mathrm{R}}_{11}(T)}{-S^{\mathrm{R}}_{11}(T_0)} \end{aligned} \tag{2.13}$$

$$t_{\mathrm{right}}(T) = S_{34'}(T) = \mathrm{e}^{-\mathrm{j}\beta_0(T)d(T)}\underbrace{S_{12}(T)\frac{1}{S^{\mathrm{L}}_{12}(T)}}_{=S_{22'}(T)} \tag{2.14}$$

Thus, the compensation is done using only measured data except for the use of the transmission factor $\mathrm{e}^{-\mathrm{j}\beta_0(T)d(T)}$, which depends on temperature through the temperature dependence of β_0 (or rather waveguide width a), and sample thickness d. The changes in a and d due to thermal expansion can be calculated from the thermal expansion coefficient for the waveguide and sample materials, respectively.

2.3 Correcting for sample displacement

Assume that the sample is displaced by a distance δ from its correct position so that the left edge is actually at $z = \delta$ and not at $z = 0$, and the right edge is actually at $z = d + \delta$ and not at $z = d$. Assuming everything else is perfect and the sample is reciprocal, we then have the reflection coefficients

$$r_{\mathrm{left}} = \mathrm{e}^{-2\mathrm{j}\beta_0\delta}r \quad \text{and} \quad r_{\mathrm{right}} = \mathrm{e}^{2\mathrm{j}\beta_0\delta}r \tag{2.15}$$

where r_{left} and r_{right} are the reflection coefficient from the left and the right, respectively. We can then find a more accurate reflection coefficient by taking the geometric mean

$$r_{\mathrm{mean}} = \sqrt{r_{\mathrm{left}}r_{\mathrm{right}}} = r \tag{2.16}$$

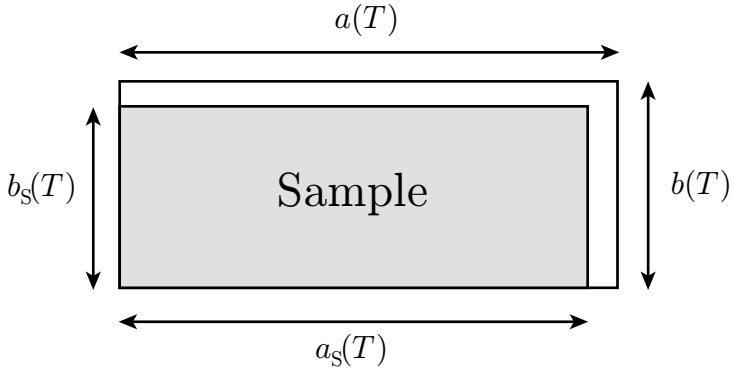

Figure 2: Drawing showing a cross section of the sample in the waveguide.

For $r_{\text{left}} - r_{\text{right}} \approx 0$ it is possible to expand (2.16) in a Taylor series

$$r_{\text{mean}} = \sqrt{r_{\text{left}} r_{\text{right}}} = \frac{1}{2}(r_{\text{left}} + r_{\text{right}}) + \mathrm{O}((r_{\text{left}} - r_{\text{right}})^2) \tag{2.17}$$

This justifies the use of the algebraic mean in the case when $r_{\text{left}} \approx r_{\text{right}}$, but the geometric mean is expected to give more accurate results. In practice, it is necessary to be careful to use the correct branch of the square root. This is achieved by assuming that $\beta_0 \delta$ is small, and compute the geometric mean as

$$r_{\text{mean}} = \sqrt{|r_{\text{left}} r_{\text{right}}|}\mathrm{e}^{\mathrm{j}(\arg(r_{\text{left}}) + \arg(r_{\text{right}}/r_{\text{left}})/2)} \tag{2.18}$$

The transmission coefficient is not influenced by a sample displacement, but we use the same geometric mean to produce an unambiguous transmission coefficient $t = \sqrt{t_{\text{left}} t_{\text{right}}}$ for the NRW inversion procedure.

2.4 Correcting for air gaps

The waveguide and the sample slab will in general differ in thermal expansion coefficients. This will not cause a problem when the assembly is heated if the sample has a larger thermal expansion coefficient than the waveguide, of course unless the strain causes the sample to crack or shatter. If the sample has a smaller thermal expansion coefficient than the waveguide then air gaps will form around the sample when the assembly is heated. This is shown in Figure 2. The air gap will introduce an error in the determined material parameters. The effect of the air gap is most severe for the gap along the horizontal edges of the sample, since the electric field is very small close to the vertical walls of the waveguide. This error increases with increasing values of ϵ and μ. The case where the sample does not fill the waveguide completely leaving an air gap has been treated by several authors. [3, 6, 7, 15, 18, 22, 25, 29].

The experimental solution of applying a conducting paste to the edges of the sample has been found to work well for room temperature measurements [3, 29]. However, this will in general not work for the high temperature measurements that are considered in this paper.

Approximate corrections for the experimentally determined complex values of $\epsilon = \epsilon' - \mathrm{j}\epsilon''$ and $\mu = \mu' - \mathrm{j}\mu''$ have been given by [3, 7, 18, 22, 25].

These corrections can be derived in a quasi-static setting, where the measured permittivity ϵ_m and permeability μ_m (the output of the NRW algorithm) correspond to the harmonic and arithmetic mean value of the sample properties ϵ_s and μ_s, and the gap properties ϵ_g and μ_g, according to

$$\epsilon_\mathrm{m} = \left(\frac{1-\Delta(T)}{\epsilon_\mathrm{s}} + \frac{\Delta(T)}{\epsilon_\mathrm{g}} \right)^{-1} \tag{2.19}$$

$$\mu_\mathrm{m} = (1-\Delta(T))\mu_\mathrm{s} + \Delta(T)\mu_\mathrm{g} \tag{2.20}$$

where $\Delta(T) = (b(T) - b_\mathrm{s}(T))/b(T)$ is the volume fraction of the air gap. Here $b(T)$ and $b_\mathrm{s}(T)$ are the temperature dependent heights of the waveguide and the sample according to Figure 2.

The harmonic mean is the result of the electric field being perpendicular to the gap, and the arithmetic mean is the result of the magnetic field being parallel to the gap, corresponding to the Wiener bounds in homogenization theory [28]. Solving for the sample parameters and assuming an air gap with $\epsilon_\mathrm{g} = \mu_\mathrm{g} = 1$ implies

$$\epsilon_\mathrm{s} = \epsilon_\mathrm{m} \frac{1-\Delta(T)}{1-\Delta(T)\epsilon_\mathrm{m}} \tag{2.21}$$

$$\mu_\mathrm{s} = \mu_\mathrm{m} \frac{1-\Delta(T)/\mu_\mathrm{m}}{1-\Delta(T)} \tag{2.22}$$

Equation (2.21) can be approximated and separated in real and imaginary parts if the imaginary part of ϵ_m is small [7, 18, 22, 25]

$$\epsilon'_\mathrm{s} = \epsilon'_\mathrm{m} \frac{1-\Delta(T)}{1-\Delta(T)\epsilon'_\mathrm{m}} \tag{2.23}$$

$$\epsilon''_\mathrm{s} = \epsilon'_\mathrm{s} \left(\frac{\epsilon''_\mathrm{m}}{\epsilon'_\mathrm{m}} \right) \frac{1}{1-\Delta(T)\epsilon'_\mathrm{m}} \tag{2.24}$$

Equation (2.22) can be separated without approximations [3, 22]

$$\mu'_\mathrm{s} = \mu'_\mathrm{m} \frac{1-\Delta(T)/\mu'_\mathrm{m}}{1-\Delta(T)} \tag{2.25}$$

$$\mu''_\mathrm{s} = \mu''_\mathrm{m} \frac{1}{1-\Delta(T)} \tag{2.26}$$

A frequency dependent approach to determine the permittivity of a nonmagnetic material in the presence of a gap is given by [3, 7, 15], based on the transverse resonance condition of a partially filled waveguide. Here we write these formulas assuming that the gap is filled with air with $\epsilon_\mathrm{g} = 1$:

$$\tan(k_1 b(T)\Delta(T)) + \chi \tan(k_2 b(T)(1-\Delta(T))) = 0 \tag{2.27}$$

Material	$\alpha[10^{-6}\,\mathrm{K}^{-1}]$
Inconel®, [13]	12.9
Macor®, [14]	11.4
Al_2O_3, [16]	7.1
Si_3N_4, [5]	3.1
SiC, [17]	4.4
NiZn ferrite, [24]	7–8

Table 1: Thermal expansion coefficients at 500°C for some materials.

where $k_1 = k_0\sqrt{1-\epsilon_\mathrm{m}}$, $k_2 = k_0\sqrt{\epsilon_\mathrm{s}-\epsilon_\mathrm{m}}$ and

$$\chi = \frac{k_2}{k_1\epsilon_\mathrm{s}} = \frac{1}{\epsilon_\mathrm{s}}\sqrt{\frac{\epsilon_\mathrm{s}-\epsilon_\mathrm{m}}{1-\epsilon_\mathrm{m}}} \tag{2.28}$$

Equation (2.27) can be solved by iteration or with a global search algorithm. Equation (2.27) reduces to equation (2.21) in the static limit as $k_0 \to 0$.

Assuming that there is no air gap at reference temperature T_0, *i.e.*, $b(T_0) = b_\mathrm{s}(T_0) = b_0$, the temperature dependent heights can be estimated by $b(T) = b_0(1 + \alpha_\mathrm{wg}(T - T_0))$ and $b_\mathrm{s}(T) = b_0(1 + \alpha_\mathrm{s}(T - T_0))$, where α_wg and α_s are the thermal expansion coefficients of the waveguide and the sample, respectively. Assuming that the waveguide expands more than the sample, the volume fraction of the airgap as a function of temperature, $\Delta(T)$, can then be calculated theoretically as

$$\begin{aligned}\Delta(T) = \frac{b(T) - b_\mathrm{s}(T)}{b(T)} &= \frac{b_0(1 + \alpha_\mathrm{wg}(T - T_0)) - b_0(1 + \alpha_\mathrm{s}(T - T_0))}{b_0(1 + \alpha_\mathrm{wg}(T - T_0))} \\ &= \frac{\alpha_\mathrm{wg} - \alpha_\mathrm{s}}{1/(T - T_0) + \alpha_\mathrm{wg}}\end{aligned} \tag{2.29}$$

Some typical values for the thermal expansion coefficients can be found in Table 1.

3 Measurements

3.1 High temperature waveguide fixture

The heated waveguide parts should be able to withstand repeated cycling from room temperature, in our case 22 °C, up to temperatures of 1000 °C according to the design criteria. Commercially available waveguide fixtures for material parameter measurements are not specified for these temperatures which means that a waveguide fixture has to be manufactured from a material that can withstand these temperatures without permanent deformation and oxidization. Furthermore it should have good thermal conductivity allowing for efficient cooling [9]. A material which meets these specifications is Inconel alloy 600® (Inconel). This is an oxidization resistant nickel-chromium-iron alloy which has low resistivity ($\approx 1\,\mu\Omega$m) for the entire temperature range. This alloy is designed for high temperature applications, *e.g.*, in

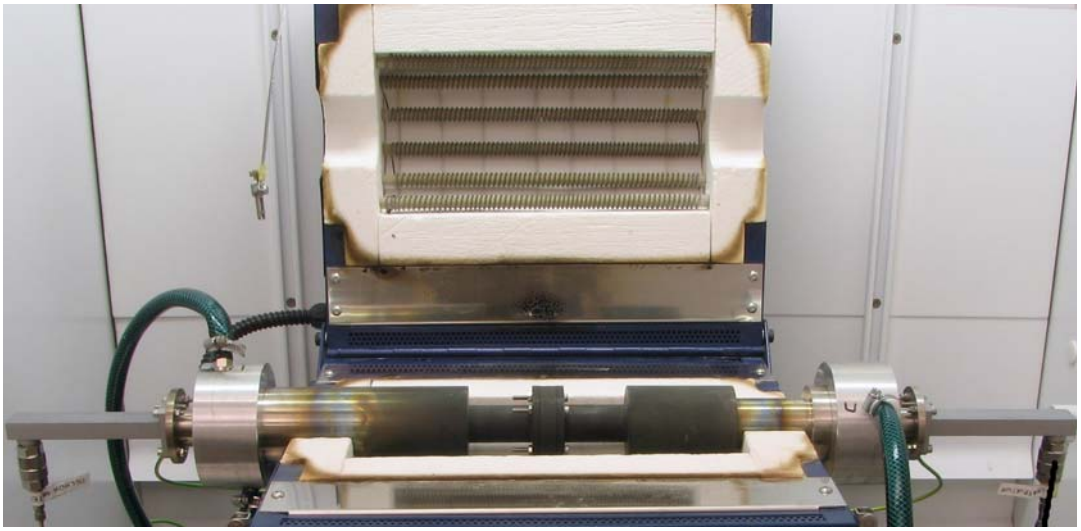

Figure 3: The figure shows the clam shell tube oven and the X-band waveguide contained in the hood. Note the cylindrical water jackets for cooling that are attached to the parts of the waveguide that are extending outside the oven.

the nuclear, aeronautic and chemical industries [13]. The thermal expansion of the material is also well known [21].

Inconel is therefore chosen for the high temperature part of the waveguide. The manufacturing of the waveguide parts is only described briefly here and more details can be found in [9]. The three parts of the waveguide fixture, the left/right parts and the sample holder are machined from cylindrical solid pieces of Inconel. The sample holder section of a standard room temperature fixture for waveguide measurements can usually be dismantled in two separate pieces simplifying the use of a tightly fitting sample slab. However, for a high temperature fixture such a design would cause deformation of the sample holder after some heating cycles. Accordingly, the sample holder in the high temperature fixture described here is made in one piece. The rectangular waveguide hole through the cylindrical piece is cut using electrical discharge machining. In addition a reflection standard is manufactured. The manufacturing process gives a waveguide with the inner dimensions $22.82 \times 10.18\,\mathrm{mm}^2$, *i.e.*, size deviations from the standard WR-90 X-band wave guide of $-0.04\,\mathrm{mm}$ in width and $+0.02\,\mathrm{mm}$ in height, respectively.

A type K thermocouple is used to measure the temperature. The thermocouple sensor is placed close to the sample in a hole drilled in the sample holder for the purpose.

The high temperature Inconel section of the assembled waveguide fixture extends outside the heating oven. Water cooling jackets are affixed to these parts of the Inconel waveguide in order to thermally separate the high temperature part of the waveguide from the room temperature waveguide parts connecting to the semi rigid microwave cables using conventional microwave connectors. The assembled waveguide fixture, including the sample holder and the cooling jackets, is seen in

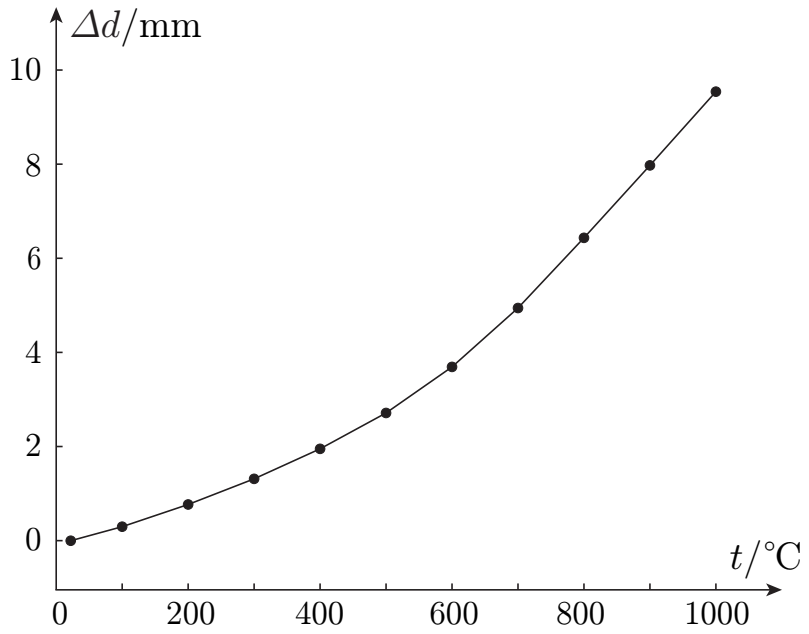

Figure 4: The figure shows the calculated displacement of the S_{21} reference plane at 10 GHz as a function of temperature. The displacement Δd is calculated from measurement data via the relation $\mathrm{e}^{-\mathrm{j}\beta_0\Delta d} = S_{21}^{\mathrm{L}}(T)/S_{21}^{\mathrm{L}}(T_0)$.

Figure 3. The clam shell oven is placed in a fume hood with good ventilation to take care of gases or fumes emitted from the sample or the oven. The airflow also provides additional cooling to the parts of the waveguide that are not heated.

The maximum temperature that can be reached is at present equal to the design maximum temperature of 1000 °C. The maximum temperature is limited by the heating power of the used oven. One measurement run, from 22 °C to 1000 °C, takes 1 h to complete. This setup could presumably be used for higher temperatures also with a more powerful oven since Inconel alloy 600® will maintain its properties at least up to 1093 °C [13].

3.2 Compensation measurements

Heating the waveguide causes it to expand and increase its length. This will cause the reference planes to move, see Section 2.2. Compensation measurements are therefore performed to record the S-parameters for the reflection and line standards at a number of temperatures as a function of frequency. The setup is first calibrated at 22 °C using a conventional waveguide TRL calibration [10] for the vector network analyzer. The S-parameters are then measured at 22 °C and at temperature increments up to the maximum temperature, 1000 °C. The acquired S-parameters are then used to compensate for the reference plane movements according to the procedure described in Section 2.2. The S_{21} reference plane displacement calculated from the compensation measurements is shown in Figure 4.

3.3 Sample measurements

The setup is first calibrated at 22 °C in the same way as for the compensation measurements. The sample slab is inserted in the sample holder taking care to align one of the sample faces with the left sample holder edge, see Figure 1. The S-parameters are measured at 22 °C and at temperature increments up to the maximum temperature, 1000 °C, or a lower temperature if desired.

When the S-parameters have been aquired the corrections are performed in the following steps:

1. Reference plane compensation. The measured S-parameters reference planes are corrected using the high temperature compensation measurement data according to the procedure described in Section 2.2. The thermal expansion in waveguide width a and sample thickness d is included in the correction.

2. Sample displacement compensation. One set of r and t parameters are then determined using the sample displacement correction procedure described in Section 2.3.

3. NRW inversion procedure. The corrected r and t parameters are used to determine ϵ and μ using the NRW method described in Section 2.1.

4. Air gap correction. Correction for the air gap between sample and waveguide caused by thermal expansion as described in Section 2.4.

Ideally, this procedure has removed all systematic errors and the remaining uncertainty in the material parameters due to noise can be given a lower bound using the Cramér-Rao bounds developed in [23].

4 Results and discussion

Measurements on Macor and NiZn Ferrite samples are performed in order to evaluate the performance of the setup and the procedure that is used to determine the permittivity and permeability from the measured S-parameters for the high temperature measurements. Macor is chosen because it is a commercially available ceramic material that is machinable to desired size and can be used for temperatures up to 1000 °C. The material has a dielectric constant of 5.67 and a dielectric loss tangent of $7.1 \cdot 10^{-3}$ at 8.5 GHz [14]. Since Macor has no magnetic properties, additional measurements are performed with a ferrite material in order to obtain results having both complex permittivity and complex permeability.

Figure 5 shows the complex permittivity and permeability determined from measurements at 300 °C for Macor. Results with and without the correction for the reference planes described in Section 2.2 are shown. This shows the necessity of the reference plane correction. Figure 4 shows that the S_{21} reference plane displacement at 10 GHz is more than 1 mm for this temperature which significantly changes the phase of the measured S-parameters and consequently the measured values of ϵ and

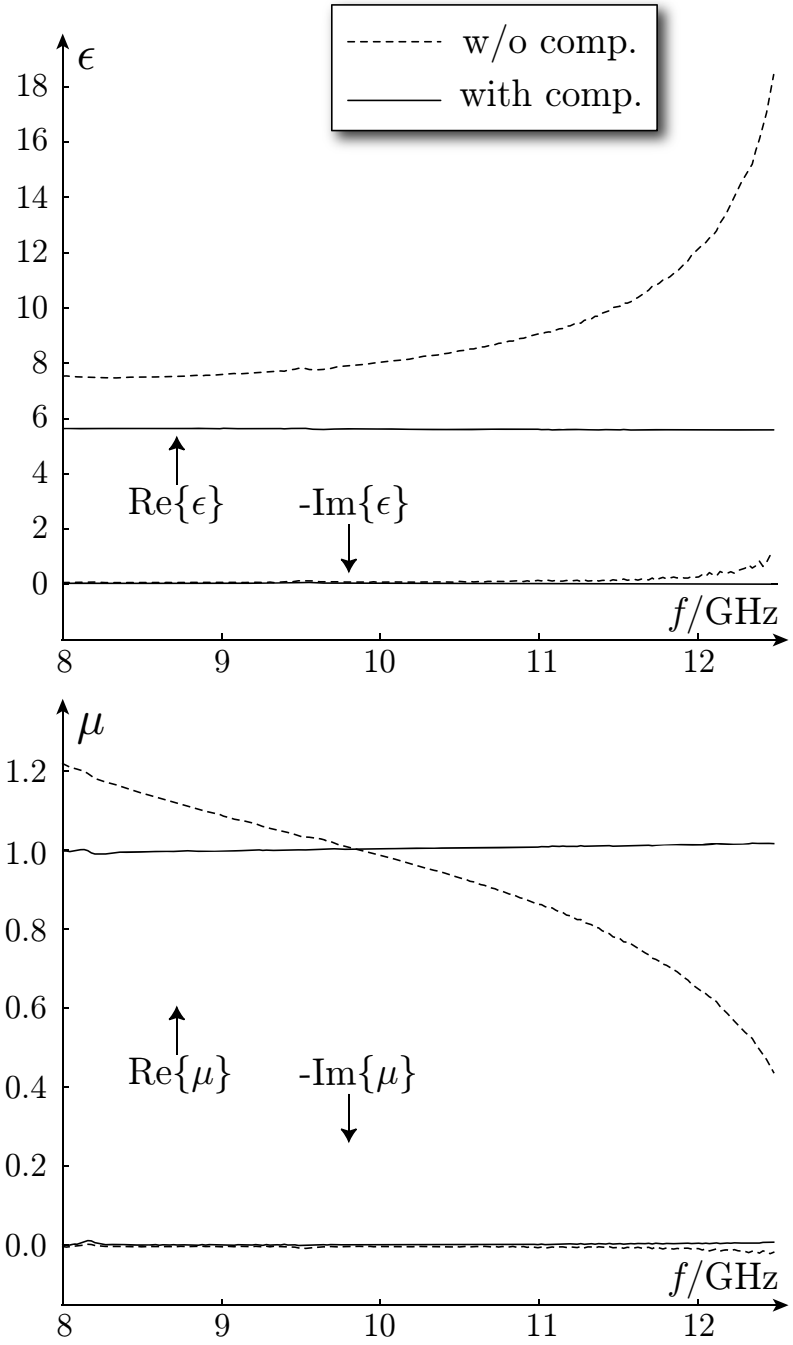

Figure 5: The complex permittivity and permeability determined from measurements at 300 °C for Macor. Results with and without the temperature compensation described in this paper are shown.

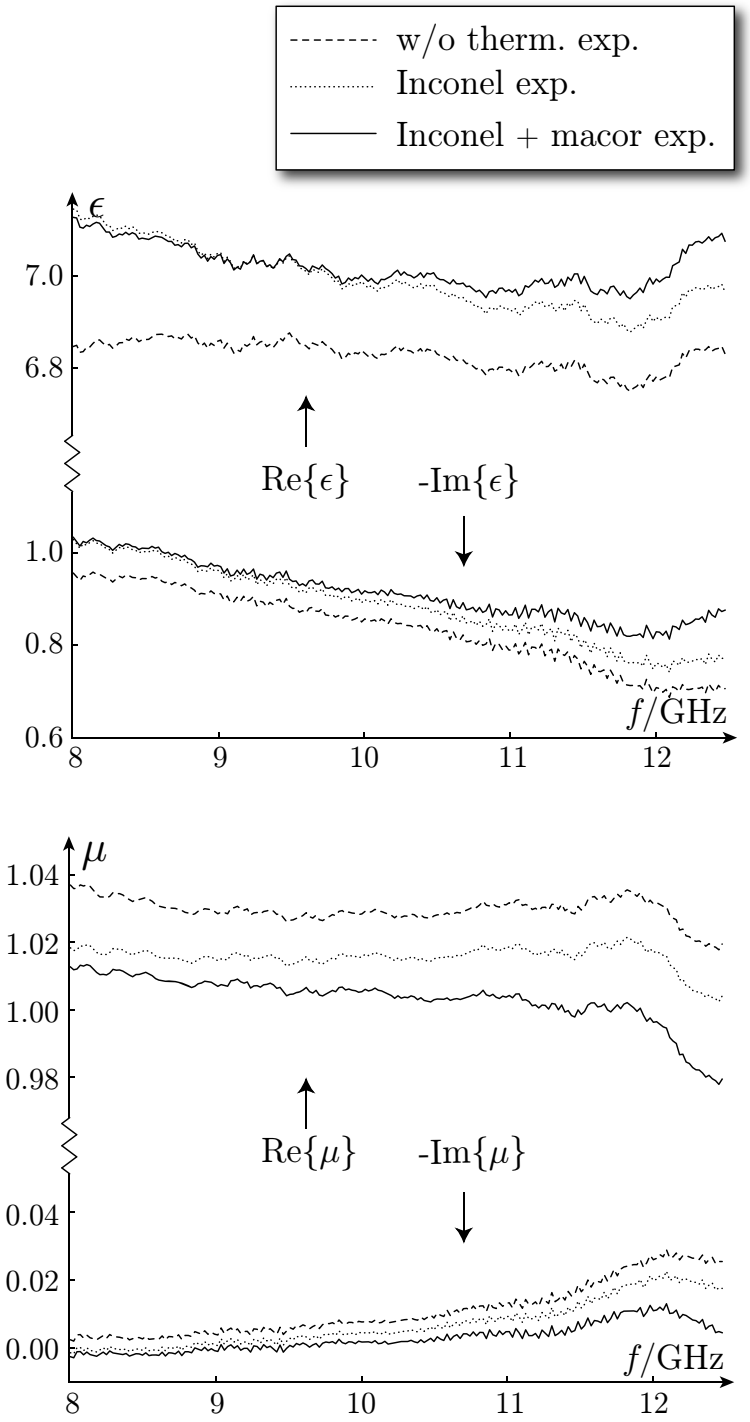

Figure 6: The complex permittivity and permeability determined at 900 °C for Macor. Results assuming no temperature dependent expansion of the waveguide width, a, and the sample thickness, d, are plotted with results assuming a temperature dependent expansion of these parameters.

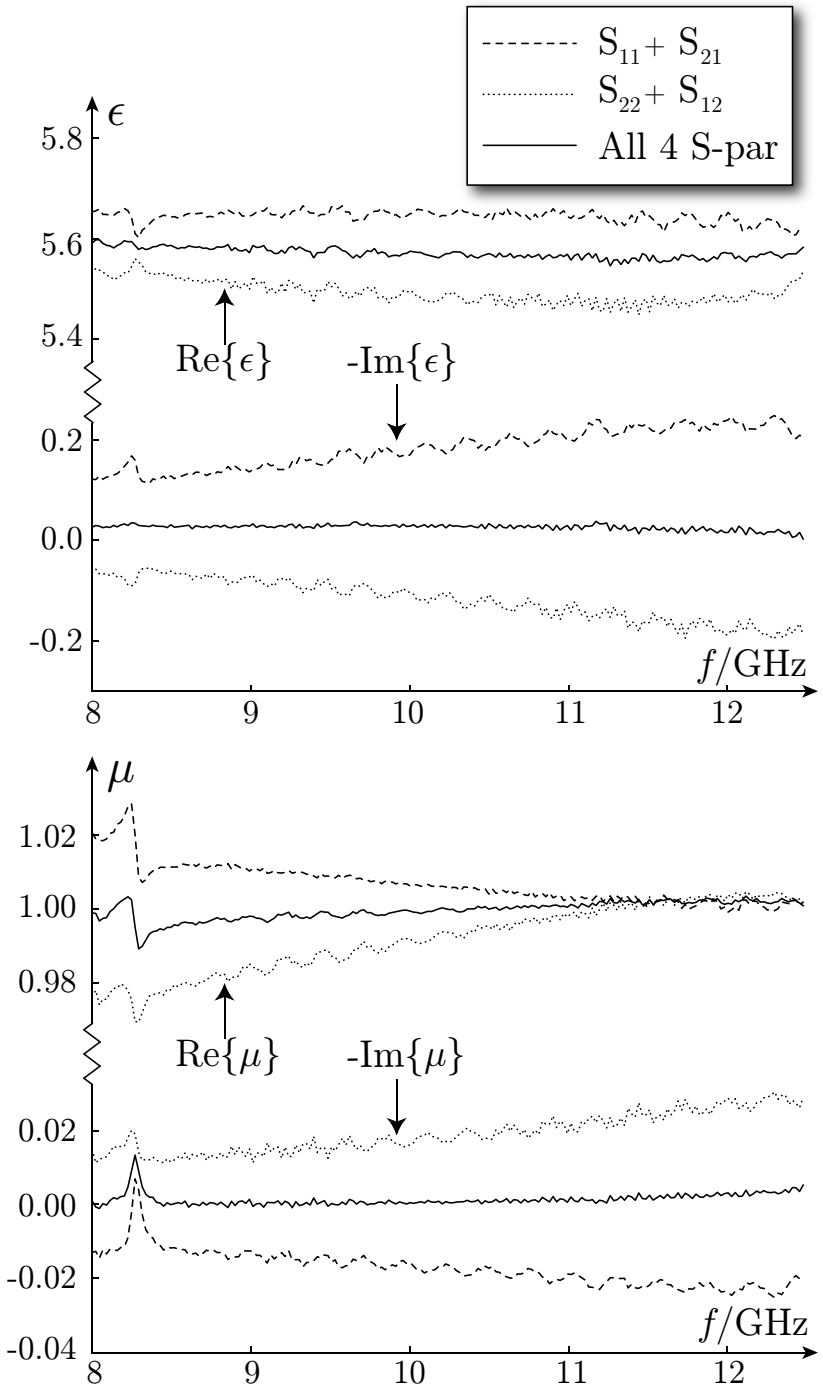

Figure 7: The complex permittivity and permeability at room temperature for Macor determined using either S_{21} and S_{11}, S_{12} and S_{22} or all four S-parameters.

μ. This is also the most important of the corrections described in this paper. Without this correction the NRW procedure even predicts a small positive imaginary part in μ as seen in Fig. 5, which is clearly unphysical.

The next question is how the thermal expansion of the waveguide width a, and the sample thickness d, influence the determined values of permittivity and permeability. This is shown in Figure 6 where it can be seen that both the expansion of a and d affect the determined parameters, although the effect is only seen after zooming in on the graphs. This means that thermal expansion in a and d should be accounted for in the correction procedure if the thermal expansion coefficients are known. In the case they are not known approximate values can be used in order to get an estimate of how much this influences the final results, and thus provides an estimate of the systematic error.

Next, we will consider the effect of a small sample displacement and how this can be corrected for. See Section 2.3 for the correction procedure. To isolate the sample displacement effect from the thermal effect this is studied at room temperature, see Figure 7. Results are shown of using only the "left" S-parameters, S_{11} and S_{21}, only the "right", S_{22} and S_{12}, or using all four S-parameters to form the reflection and transmission coefficients, r and t, used in the NRW inversion procedure. The sample displacement correction procedure has the effect to average out the frequency dependence, caused by a small sample position offset, as well as to average out some of the noise in the results.

Having performed the correction for the reference planes, the waveguide expansion in width and the displacement of the sample one can analyze the permittivity and permeability dependence on temperature. Figure 8 shows these parameters as a function of temperature at 10 GHz. The result without gap correction is shown with black symbols. The effect of an air gap due to that the thermal expansion coefficient is smaller for Macor than for Inconel is also determined using (2.21)–(2.28). The two quasi-static expressions for the air gap correction in (2.23)–(2.24) and (2.21) give very similar results for this case. This is shown with gray symbols in Figure 8. The white symbols show the temperature dependence after a gap correction using the frequency dependent method in (2.28). The air gap corrections have some effect on the permittivity values, especially at the higher temperatures and larger values of the permittivity, while the permeability is left relatively unaffected with an almost complete overlap between the permeability curves before and after gap correction in Figure 8. There is also some difference between the quasi-static and the frequency dependent gap corrections.

The results presented here can be compared with a previous study where the complex permittivity for Macor as a function of temperature is measured at 2.45 GHz for the temperature range up to 800 °C using a coaxial surface probe [1]. The qualitative agreement between the results in [1] and the results presented in the present study is good with the typical "two-stage" shape in the curve showing the permittivity as a function of temperature, *i.e.*, the slope of the curve changes at a temperature of 500 °C. Quantitatively, there are some differences which may be expected when comparing measurements from different frequency ranges. The real part of the permittivity increases from 6.0 to 8.0 and the imaginary part increases

from 0.21 to 1.85 as the temperature is raised from room temperature to 800 °C in [1]. The corresponding increases for the measured values in the present study are from 5.6 to 6.9 for the real part and from 0.028 to 1.5 for the imaginary part of the permittivity.

Figure 9 shows the complex permittivity and permeability as a function of frequency determined at 22 °C and 300 °C for the ferrite sample. The data has here been corrected for the sample displacement, displacement of the reference planes, waveguide and sample expansion and for the air gap that forms as the temperature increases. The real part of the permittivity is smaller for the higher temperature while the imaginary part is larger. The real part of the permeability is similar for the two temperatures while the imaginary part is larger for 300 °C than for 22 °C.

Figure 10 shows the complex permittivity and permeability for a ferrite sample determined at 10 GHz as a function of temperature. The black symbols show the results without a temperature air gap correction. The gray and white symbols show the results after a gap correction using the quasi-static expressions in (2.23)–(2.24) and (2.21), respectively. The temperature dependence for this sample is completely different compared with the Macor sample. The ferrite electromagnetic parameters as a function of temperature are smooth at relatively low temperature, but an irreversible change takes place at temperatures above 400 °C. The DC resistance of the sample is also reduced when measured with a simple ohmmeter after the experiment compared to before the heating, indicating that the material has become electrically conducting after being heated. The behavior of the electromagnetic parameters at temperatures above 400 °C is consistent with a material that has very good conductivity and very low transmission through the sample. One can compare with a perfect electrical conductor (PEC) material which is reached in the limit $\epsilon \to \infty$ and $\mu \to 0$.

Future development plans for the high temperature setup that is described in this paper include the construction of rectangular waveguides suitable for measurements in other frequency bands. A coaxial line fixture for wideband measurements is another useful addition that is more technically challenging due to the necessity to construct a connection to the sample holder center connector that can withstand high temperatures.

5 Conclusions

A single waveguide setup is developed for the measurement of permittivity and permeability at temperatures up to 1000 °C. The thermal expansion of the waveguide and the sample are corrected for by a reference plane compensation, compensation for the expansion of the waveguide width a and sample thickness d, and displacement of sample. The corrected reflection and transmission parameters are then used in an NRW inversion procedure, and a final correction for temperature dependent air gap is made. With no air gap compensation, the measured permittivity is usually underestimated. The setup and the compensation procedures are tested on measurements on samples of Macor and NiZn ferrite.

It is concluded that a rectangular X-band single waveguide setup can be used for measurements of the permittivity and permeability from room temperature up to

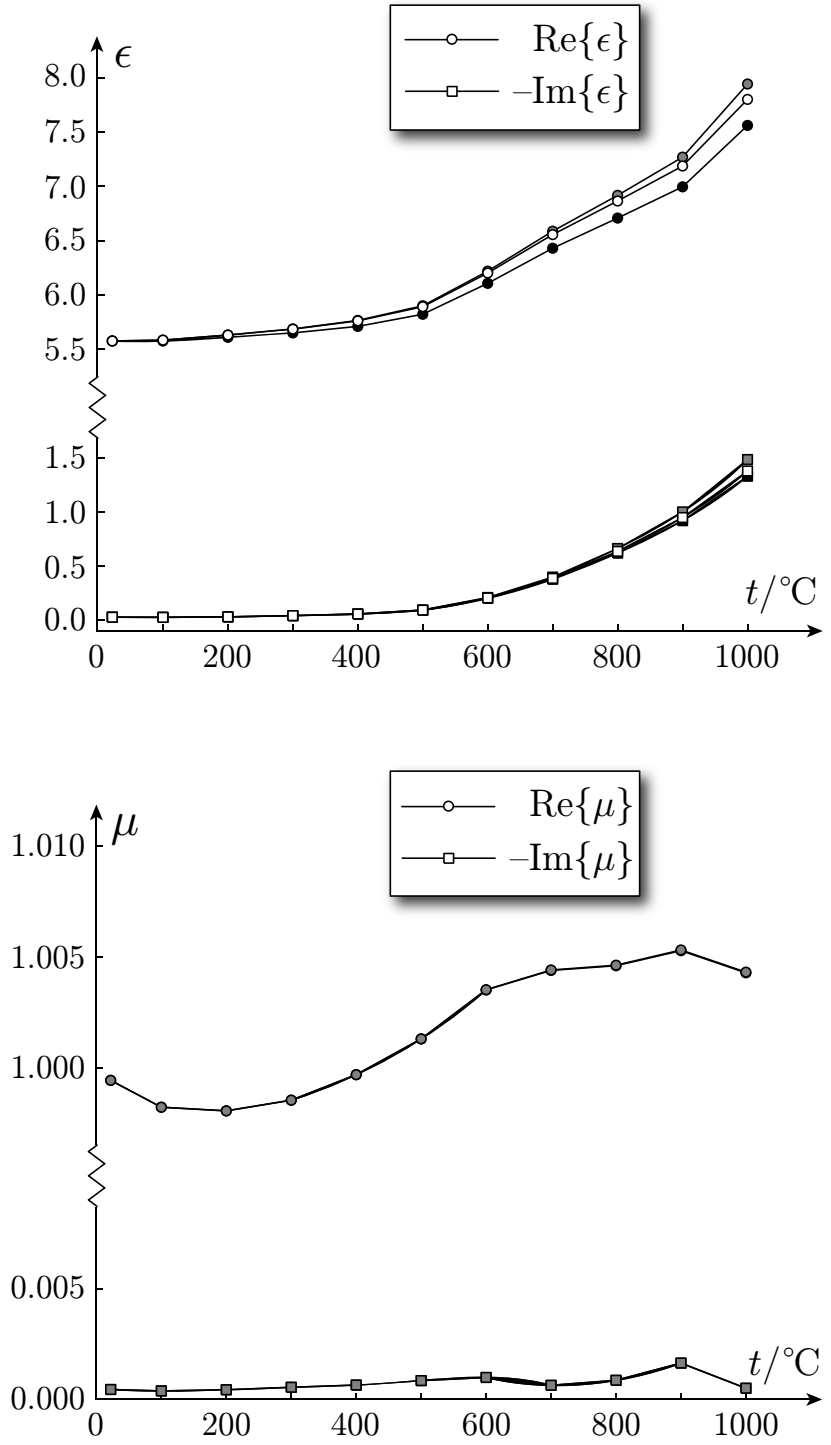

Figure 8: The complex permittivity and permeability at 10 GHz as a function of temperature for Macor. The black symbols show the results without a temperature air gap correction, the gray symbols show the results using the quasi-static air gap correction, and the white symbols show the results using the frequency dependent air gap correction.

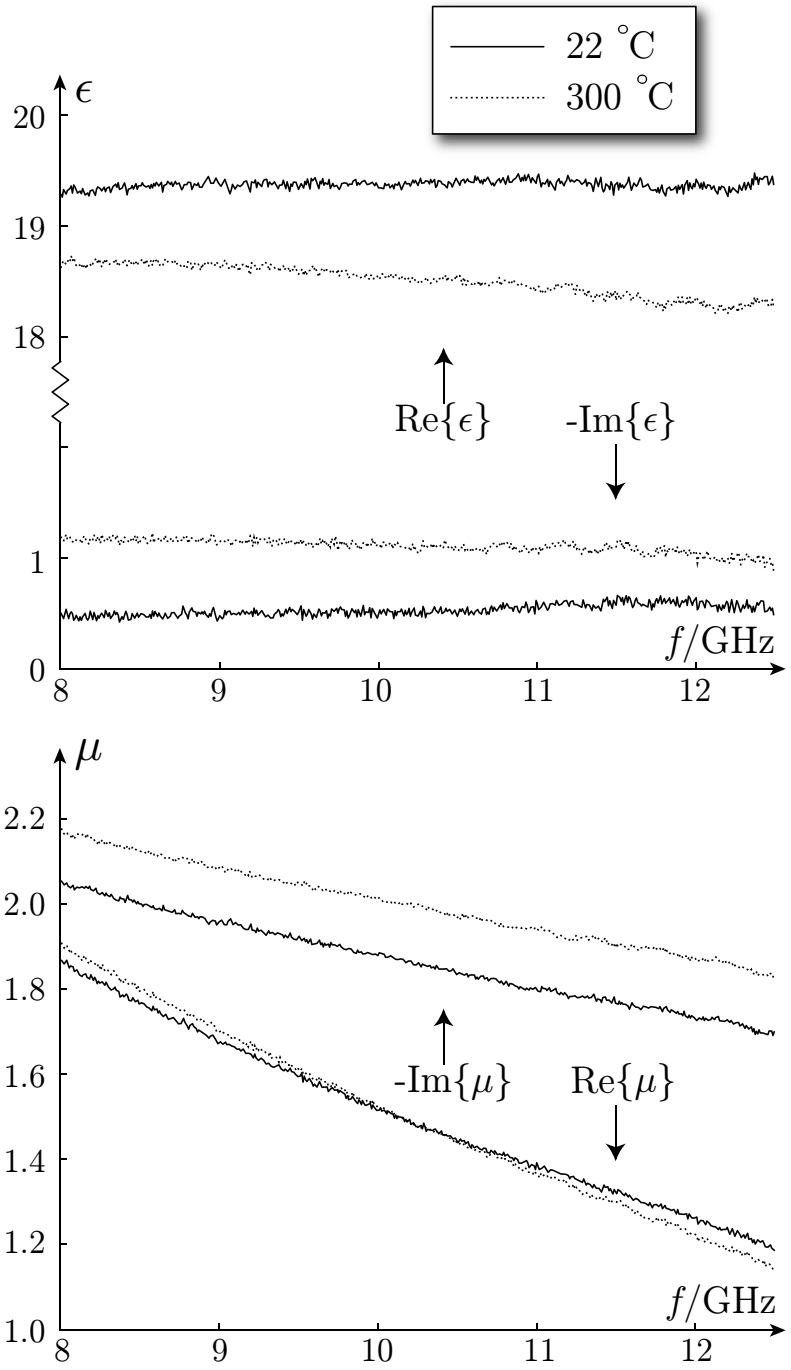

Figure 9: The complex permittivity and permeability as a function of frequency determined at 22 °C and 300 °C for a ferrite sample. The data has been corrected for the sample displacement, displacement of the reference planes, waveguide thermal expansion, sample thermal expansion and the temperature dependent air gap.

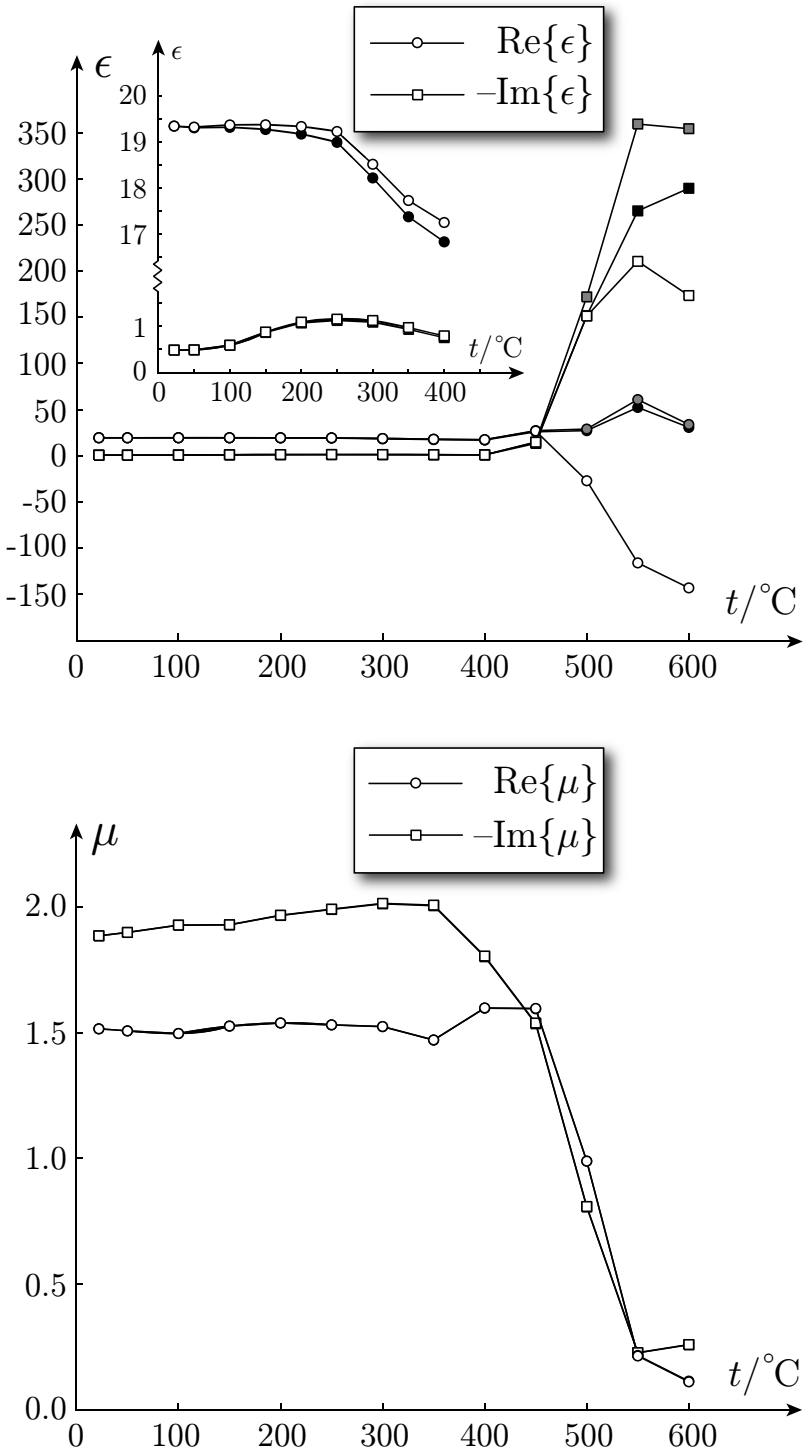

Figure 10: The complex permittivity and permeability for a ferrite sample determined at 10 GHz as a function of temperature. The black symbols show the results without a temperature air gap correction, the gray symbols show the results after gap correction using (2.23)–(2.24), and the white symbols show the results after gap correction using (2.21).

1000 °C. Future development includes rectangular waveguides for other bands and a coaxial line fixture for wideband measurements.

Acknowledgments

The financial support by the Swedish Foundation for Strategic Research through Strategic Mobility grants, and the Swedish Defense Materiel Administration, is gratefully acknowledged. We would also like to acknowledge the technical assistance from Mats Andersson and Karin Brage at Saab Bofors Dynamics.

References

[1] M. Arai, J. G. P. Binner, G. E. Carr, and T. E. Cross. High temperature dielectric measurements on ceramics. In *Sixth International Conference on Dielectric Materials, Measurements and Applications, 1992*, pages 69–72, 1992.

[2] J. Baker-Jarvis, R. G. Geyer, and P. D. Domich. A nonlinear least-squares solution with causality constraints applied to transmission line permittivity and permeability determination. *IEEE Trans. Instrumentation and Measurement*, **41**(5), 646–652, 1992.

[3] J. Baker-Jarvis, M. D. Janezic, J. H. Grosvenor, Jr., and R. G. Greyer. Transmission/reflection and short-circuit line methods for measuring permittivity and permeability. Technical Report Tech. Note 1355-R, National Institute of Standards and Technology, National Institute of Technology, 325 Broadway, Boulder, CO 80303-3328, 1993. `http://www.nist.gov`.

[4] J. A. Batt, R. Rukus, and M. Gilden. General purpose high temperature microwave measurement of electromagnetic properties. In R. L. Beatty, W. H. Sutton, and M. F. Iskander, editors, *Materials Research Society Symposium Proceedings*, volume 269, pages 553–559, Pittsburgh, PA, 1992. Materials Research Society.

[5] J. Blumm. Optimizing silicon nitride ceramics. *Ceramic Industry*, pages 23–28, feb 2004. http://www.ceramicindustry.com.

[6] K. S. Champlin and G. H. Glover. "Gap effect" in measurement of large permittivities. *IEEE Trans. Microwave Theory Tech.*, **MTT-14**, 397–398, 1966.

[7] L. F. Chen, C. K. Ong, C. P. Neo, V. V. Varadan, and V. K. Varadan. *Microwave electronics: Measurement and materials characterisation*. John Wiley & Sons, New York, 2004.

[8] D. Couderc, M. Giroux, and R. G. Bosisio. Dynamic high temperature microwave complex permittivity measurements on samples heated via microwave absorption. *Journal of Microwave Power*, **8**(1), 69–82, 1973.

[9] L. Elmkvist. Waveguide measurements at high temperatures. Master's thesis, Chalmers University of Technology, Department of Applied Physics, SE-412 96 Gothenburg, Sweden, 2007. In cooperation with Saab, Linköping, Sweden.

[10] G. F. Engen and C. A. Hoer. "Thru-Reflect-Line": An improved technique for calibrating the dual six-port automatic network analyzer. *IEEE Trans. Microwave Theory Tech.*, **27**, 987–993, 1979.

[11] N. H. Harris, J. R. Chow, R. L. Eisenhart, and B. M. Pierce. Dielectric properties of ceramics at microwave frequencies. In *Ceramic transactions. Proceedings of the symposium on microwave theory and application in materials*, volume 21, pages 235–242. American Ceramic Society, 1991.

[12] W. W. Ho. High-temperature dielectric properties of polycrystalline ceramics. In W. H. Sutton, M. H. Brooks, and I. J. Chabinsky, editors, *Microwave processing of materials, Materials research society symposia proceedings*, volume 124, pages 137–158. Materials Research Society, 1988.

[13] Inconel alloy 600 data sheet. http://www.specialmetals.com, 2010.

[14] Macor product information sheet. http://www.corning.com, 2010.

[15] N. Marcuvitz. *Waveguide Handbook*. McGraw-Hill, New York, 1951.

[16] R. G. Munro. Evaluated material properties for a sintered α-alumina. *J. Am. Ceram. Soc.*, **80**(8), 1919–28, 1997.

[17] R. G. Munro. Material properties for a sintered α-SiC. *J. Phys. Chem. Ref. Data*, **26**(5), 1195–1203, 1997.

[18] J. Musil and F. Zacek. *Microwave Measurements of Complex Permittivity by Free Space Methods and their Applications*. Elsevier Science Publishers, Amsterdam, 1986.

[19] National Research Council (U.S.). Committee on Microwave Processing of Materials: An Emerging Industrial Technology. *Microwave processing of materials*. National Academy Press, Washington, D.C., 1994.

[20] A. M. Nicolson and G. F. Ross. Measurement of the intrinsic properties of materials by time-domain techniques. *IEEE Trans. Instrumentation and Measurement*, **19**, 377–382, 1970.

[21] S. Raju, K. Sivasubramanian, R. Divakar, G. Panneerselvam, A. Banerjee, E. Mohandas, and M. P. Antony. Thermal expansion studies on Inconel-600(R) by high temperature X-ray diffraction. *Journal of Nuclear Materials*, **325**(1), 18–25, 2004.

[22] *Measurement of dielectric material properties. Application Note.* Rohde & Schwarz, Systems & Communications Asia Pte Ltd, 1 Kaki Bukit View, Singapore 415941, 2006. `http://www2.rohde-schwarz.com`.

[23] D. Sjöberg and C. Larsson. Cramér-Rao bounds for determination of permittivity and permeability in slabs. Technical Report LUTEDX/(TEAT-7190)/1–13/(2010), Lund University, Department of Electrical and Information Technology, P.O. Box 118, S-221 00 Lund, Sweden, 2010. http://www.eit.lth.se.

[24] Soft ferrites — ferrite materials survey. http://www.ferroxcube.com, 2008.

[25] M. Sucher and J. Fox. *Handbook of microwave measurements*. Interscience, New York, 3. ed. edition, 1963.

[26] V. V. Varadan, R. D. Hollinger, D. K. Ghodgaonkar, and V. K. Varadan. Free-space, broadband measurements of high-temperature, complex dielectric properties at microwave frequencies. *IEEE Trans. Instrumentation and Measurement*, **40**(5), 842–846, 1991.

[27] W. B. Weir. Automatic measurement of complex dielectric constant and permeability at microwave frequencies. *Proc. IEEE*, **62**, 33–36, 1974.

[28] O. Wiener. Die Theorie des Mischkörpers für das Feld des stationären Strömung. *Abh. Math. -Physichen Klasse Königl. Sächs. Gesel. Wissen*, **32**, 509–604, 1912.

[29] S. B. Wilson. Modal analysis of the "Gap effect" in waveguide dielectric measurements. *IEEE Trans. Microwave Theory Tech.*, **36**(4), 752–756, 1988.